J Electroceram (2007) 18:197–204
DOI 10.1007/s10832-007-9026-5

Dispersion and rheology of $BaTiO_3$ nanoparticles in ethanol–isopropanol solvents

Wenjea J. Tseng · Shin-Ru Wang

Received: 14 July 2006 / Accepted: 15 September 2006 / Published online: 13 March 2007

Abstract Barium titanate ($BaTiO_3$) nanoparticles were dispersed in ethanol–isopropanol mixtures and their rheological behaviors were examined in terms of surfactant concentration (0–5 wt.% of the solids) and volumetric solids loading ($\phi = 0.10 - 0.35$) over a shear-rate ($\dot{\gamma}$) range 1 to 1,000 s^{-1}. An oxyethylene-based polymeric surfactant was used to facilitate the nanoparticle dispersion. A pronounced viscosity reduction, >95% when compared to the suspensions without the dispersant, resulted with a surfactant concentration of 4 wt.% at a constant shear rate of 100 s^{-1}. This finding was in parallel with a simultaneous reduction in the mean "floc" size of the suspensions. Shear-thinning flow character resulted over most of the shear-rate range examined, especially for the concentrated suspensions with $\phi \geq 0.25$. The concentrated suspensions were indeed flocculated. This increased instability was partly due to the compression of electrical double layer as the particulate solids became more crowded in the carrier solvents, and also to the increased "effective" solids concentration because of the preferential adsorption of the surfactant molecules on the nanoparticle surface.

Keywords Barium titanate · $BaTiO_3$ · Agglomeration · Nanoparticle · Rheology

W. J. Tseng (✉) · S.-R. Wang
Department of Materials Engineering,
National Chung Hsing University,
250 Kuo Kuang Road,
402 Taichung, Taiwan
e-mail: wenjea@dragon.nchu.edu.tw

1 Introduction

Barium titanate ($BaTiO_3$) has been used extensively in multilayer ceramic capacitors (MLCCs) for microelectronics and wireless communication devices that require advanced properties of high frequency, high volumetric efficiency and high reliability [1–3]. The applications often involve processing of $BaTiO_3$ powders into thick-film forms; to which, the $BaTiO_3$ powders are mixed with organic solvent or water to form uniform suspensions before being shaped under shear by tape casting [2–4]. A successful tape casting often requires a low-viscous slurry with a high solids loading at high shear rates for the ease of shape-forming, while the suspension needs to provide a suitable yield stress to keep the shape attained during the removal of forming stress [5]. Minor addition of organic surfactant is often used in practice to achieve the required flow properties of the slurry, and the influence of surfactant to the overall suspension stability has attracted much attention in the literature [6–18].

A stable powder suspension may be rendered by careful control of the interparticle potentials in liquid; from which, an optimal interparticle repulsion via electrostatic and/or steric hindrance mechanism is beneficial [5–7, 16, 18]. This implies that the interparticle attraction arising from the van der Waals force needs to be suppressed to a satisfactory low level. One generally regards the steric hindrance as a critical factor, outweighing the electrostatic effect, in providing a sufficient barrier layer to inhibit the interparticle aggregation when non-aqueous liquid is used as the solvent vehicle for tape-casting process [5, 16]. The steric mechanism involves preferential adsorption of the polar end of surfactant molecules onto particle surface, while the tail end of molecules stretches toward liquid medium to provide

the desired interparticle repulsion. The surfactants known to be effective for the dispersion of $BaTiO_3$ powders in non-aqueous media often bear excess electrical charge at one end of the molecular chain to offer an additional electrostatic repulsion in addition to the steric effect for an improved dispersion/stabilization [7–11]. Among the surfactants reported, Chartier et al. [7] used phosphate ester as a surfactant for the dispersion of $BaTiO_3$ in 2-butanone: ethanol mixtures. They found that the dissociation of ester molecules in the given solvent system was critically important to the dispersion efficiency. Fowkes and Mostafa [8] proposed that the stability of $BaTiO_3$ slurries was facilitated through proton and electron exchanges at the interface of the particle surface and the suspending media. Mikeska and Cannon [9] also suggested the phosphate ester would adsorb preferentially on $BaTiO_3$ surface as a neutral molecule, which then transfers a proton to the basic site on the surface, creating a positively charged particle for the desired electrostatic repulsion. Paik et al. [10] further examined the rheology and electrokinetic characteristic of $BaTiO_3$ powders dispersed in different organic liquids (including ethanol, acetone, toluene and the mixture of these solvents) when either phosphate ester or menhaden fish oil was used as a dispersant. Solvent polarity and the electrostatic charge potential developed on the particle surface were found to influence the suspension stability in the organic liquids of low dielectric constant.

While the exact dispersion mechanisms involved in $BaTiO_3$-organic solvents-surfactant system is material and process dependent [7–10], a detailed examination about the suspension stability and the resulting rheological behavior over a broad range of solids loading and surfactant concentration is far from extensive. This paper hence focuses on the particulate dispersion and rheology of $BaTiO_3$ nanoparticle suspensions when ethanol and isopropanol solvents are used as the carrier liquid. A polymeric surfactant of non-ionic nature is used in the study to facilitate the nanoparticle dispersion, and the effect of surfactant adsorption and the solids concentration to the rheological behavior and interparticle interaction of the suspensions is discussed.

2 Experimental procedure

Hydrothermally prepared $BaTiO_3$ nanoparticles (Titanex Corp., Taiwan) with an average particle size of 60 nm were used as the raw material. From a field-emission scanning electron microscopy (FE-SEM, JSM-6700F, JEOL, Japan), the nanoparticles are mostly spherical and polygonal in shape (Fig. 1), reflecting in part the cubic symmetry of crystalline $BaTiO_3$. Reagent-grade ethanol and isopropanol (both from Sigma Chemicals, USA) were used as the solvent carrier without further purification. The solvent mixtures were prepared in a 1:1 ratio before addition of the $BaTiO_3$ nanoparticles to form powdered suspensions with volumetric solids concentrations (ϕ) ranging from 10 to 35 vol.%.

The polymeric surfactant used was non-ionic in character (Hypermer KD-6, ICI Surfactant, UK) and was an oxyethylene-based complex mixture with high amount of propylene glycol as a by-product. The surfactant concentration was up to 5% of the solids weight. All the powder suspensions were ball-mixed in polyethylene bottles for a period of 24 h before their viscosity (η_s) was determined by a strain-controlled concentric viscometer (VT550, Gebruder HAAKE Gmbh, Germany) equipped with a sensor system (MV-DIN 53019, HAAKE, Germany) of a cone-cup geometry operated at a constant temperature (25 °C). The measurement was performed with a steady increment of shear rate ($\dot{\gamma}$); to which, the rate was increased in every 1 s^{-1} over the shear-rate range of 1–10 s^{-1}, every 10 s^{-1} over 10–100 s^{-1} and every 100 s^{-1} over 100–1,000 s^{-1} [14].

Zeta potential and "floc" size of the nanoparticle suspensions were measured by an electrokinetic light-scattering technique (Zetasizer NS, Malvern Instruments, UK) at various solids concentrations. The powdered suspensions after ball-mixing were first centrifuged at a rotational speed of 10,000 rpm for 20 min. The supernatants were then carefully siphoned out by a glass pipette and then mixed with a few drops of the original, uncentrifuged suspensions to form "uniform" dispersions via an additional ultrasonic agitation (Sonicator 3000, Misonix, USA) with a power amplitude of 600 Watts operated at 20 kHz for 10 min at a constant temperature (25 °C). This operation ensures that the particles in a dilute concentration (~0.005%) were able to migrate under an applied electrical field in a liquid environment identical to the "original"

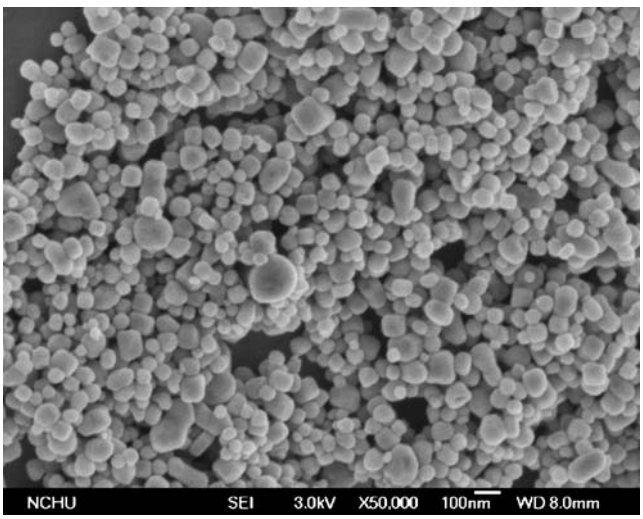

Fig. 1 Morphology of the $BaTiO_3$ nanoparticles

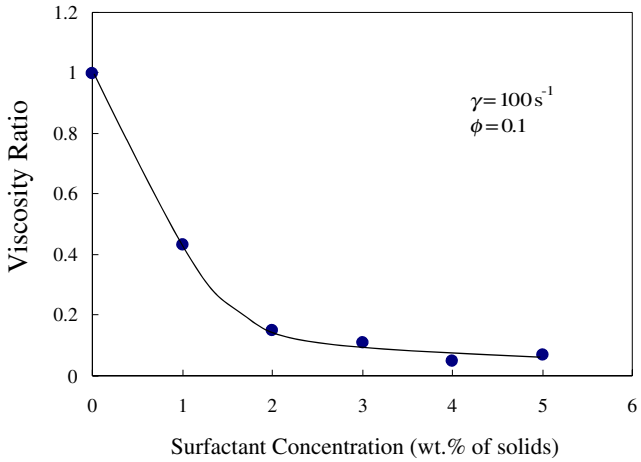

Fig. 2 Viscosity ratio at various surfactant concentrations. The solids concentration of the $BaTiO_3$ nanoparticle suspensions was held at ϕ= 0.1 and the shear rate at $\dot{\gamma} = 100\ s^{-1}$

suspensions that consist of actually higher fractions of the particulate solids.

Infrared spectra were obtained on a Perkin-Elmer RXI Spectrometer using the KBr method in the diffuse reflectance mode. The $BaTiO_3$ suspensions were dried in an oven (60 °C for 48 h), washed vigorously with additional 20 ml aliquots of ethanol–isopropanol solvents and then centrifuged at 10,000 rpm for the preparation of FT-IR samples. The washing process was repeated for four times to ensure the attained spectra were free from bands arising from residual, un-adsorbed surfactant molecules. The washed granules were dried at 60 °C and stored in desiccators until use.

Some of the nanoparticle suspensions prepared were repeatedly centrifuged at a rotational speed of 10,000 rpm and ultrasonically washed in fresh ethanol–isopropanol solvent for more than five times before the centrifuged cakes were oven-dried at ~60 °C for 48 h to remove the liquid solvent. Thermogravimetric analysis (Pyris Diamond TG/DTA, Perkin Elmer, USA) with a precision of 0.2 mg was then conducted on the dried granules at temperatures up to 600 °C in air with a heating rate of 10 °C/min. This was used to determine the amount of surfactant molecules that adhere to the particle surface in the solvent mixture. A weight loss versus the centrifugal times was conducted for the suspension with 5 wt.% surfactant addition prior to the thermogravimetric practices. The surfactant polymer began to decompose at temperature above 250 °C in air atmosphere. Fully removal of the polymeric surfactant was attained before temperature reached 600 °C. A "final" weight loss (calculated from the weight taken at 600 °C to compare with the original weight before the thermal pyrolysis) decreased as the number of centrifugation increased and began to reach a minimum as the centrifugal number exceeded three times. The weight loss was literally unchanged after three centrifugal treatments. Five centrifugal cycles were then chosen and carried out throughout the study. The adsorbed surfactant amounts on the powder surface were then determined experimentally, rendering a calculation of isothermal adsorption isotherm of the surfactant molecules on the $BaTiO_3$ particle surface.

3 Results and discussion

3.1 $BaTiO_3$ dispersion with the surfactant addition

Viscosity of the nanoparticle-filled suspensions depends critically on the polymeric surfactant concentration. In Fig. 2, viscosity ratio reduces by more than 80% as the surfactant concentration reaches 2 wt.% of the solids. The viscosity ratio then levels off gradually to a minimum of 5% as the surfactant concentration further increased. Figure 3 shows the adsorption isotherm of the surfactant molecules on the $BaTiO_3$ nanoparticle surface in ethanol–isopropanol solvents. The adsorption occurs when the polymeric surfactant is lightly added (~1 wt.%), indicating a relatively strong affinity of the surfactant molecules to specific adsorption sites available on the polar $BaTiO_3$ surface. When the adsorbed polymer molecules of sufficient thickness, distribution density, and mechanical strength are formed on the particle surface, stable suspensions can be rendered via an induced steric repulsion as the particles approach one another at a separation distance less than twice the adlayer thickness (δ). In this regard, the adsorption isotherm compares quite favorably with the viscosity result (Fig. 2). The increase in specific adsorption yet slows (in magnitude) as the surfactant concentration exceeds 1 wt.%, and this becomes more apparent as the surfactant concentration approaches toward the higher end (7 wt.%). A saturation plateau is not found over the surfactant concentration examined, indicating possible

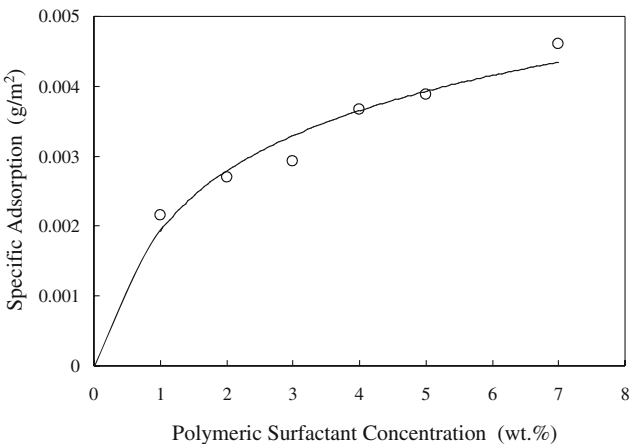

Fig. 3 The adsorption isotherm of polymeric surfactant (KD-6) on $BaTiO_3$ nanoparticles in ethanol-isopropanol solvent mixtures

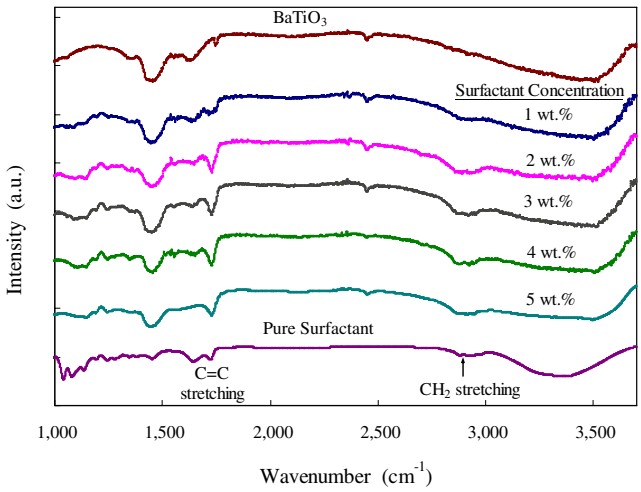

Fig. 4 FT-IR spectra of pure $BaTiO_3$, KD-6 surfactant, and $BaTiO_3$-surfactant mixtures of various concentrations

multilayer adsorption of surfactant molecules with thickness greater than the Langmuir-typed "monolayer" coverage due presumably to molecular interactions between the surfactant molecules in given carrier solvent and/or at the solid-surfactant interface. In comparison, the viscosity ratio ceases to reduce further over the same concentration range. The adsorbed molecules hence did not bridge themselves into a continuous particulate network considerably, nor did the possible change of molecular conformation with the increasing polymer molecules have any substantial effect on the macroscopic flow resistance over the surfactant concentrations examined.

Figure 4 shows the infrared spectra of the pure $BaTiO_3$, the polymeric surfactant, and the surfactant-mediated, dried $BaTiO_3$ powder mixtures. The broad band at approximately 3,200–3,600 cm^{-1} is attributable to the OH stretching vibration due to H_2O and hydroxyls on the particle surface. The small bands at 2,400 and 1,760 cm^{-1}, and the band at 1,400 cm^{-1} correspond to carbonates formed by carbon dioxide in air [19]. $BaTiO_3$ has been reported to present absorption bands at 472 cm^{-1} due to $Ti–O_{II}$ bending normal vibration, and at 615 cm^{-1} because of inter-connecting TiO_6 octahedra and $Ti–O_I$ stretching normal vibration [19, 20]. These peaks are unfortunately not found in our study due mainly to the low signal-to-noise ratio in the low wavenumbers range. However, distinctive absorption bands that are neither associated with the $BaTiO_3$ nor are those from the air atmosphere are found at 1,720 and 2,880 cm^{-1} which characterize the C=C and C–H stretching modes of the polymeric surfactant, respectively. Relative intensity of the C=C and C–H bands appears to become more pronounced when the surfactant concentration is increased above ~2 wt.%. Note that a repeated washing practice was carried out for the preparation of IR samples; therefore, the attained spectra are believed to those belonging to the surfactant molecules that anchored strongly on the nanoparticle surface in the given solvents carrier.

The mean "floc" size of the suspensions reduces rather monotonously with the increasing surfactant concentration (Fig. 5). This indicates that the surfactant addition has indeed facilitated the agglomerate breakdown in the suspensions so that the flow unit is reduced, hence allowing for the suspensions to deform at a reduced shear force under given shear rate. The decreasing trend in Fig. 5 appears to resemble the reduction of viscosity ratio in Fig. 2. An "end-point" floc size of ~160 nm is determined experimentally by the dynamic light-scattering technique from the dilute $BaTiO_3$ suspensions ($\phi \sim 0.005\%$). This floc size is substantially greater than the discrete size of $BaTiO_3$ (~60 nm) found in Fig. 1, even though the method involved in the size determination is quite different so that some uncertainties exist. Nonetheless, this suggests that "hard" $BaTiO_3$ aggregates persistently exist in the suspensions to a certain extent even with the surfactant addition.

3.2 Rheological behavior of $BaTiO_3$ nanoparticle suspensions

Figure 6 shows flow curves of the $BaTiO_3$ nanoparticle suspensions. The surfactant concentration was held at 3 wt. % of the solids for all the solids concentrations examined. At low solids concentrations ($\phi \leq 0.2$) and shear rates, shear stress (τ) appears to behave linearly proportional to shear rate ($\dot{\gamma}$) with a negligible yield stress (τ_y), revealing a Newtonian fluid with a good dispersion quality. The curves ($\phi \leq 0.2$) then deviate from the linearity at high shear rates ($\dot{\gamma} \geq \sim 600\ s^{-1}$) to change into a shear-thickening flow. This

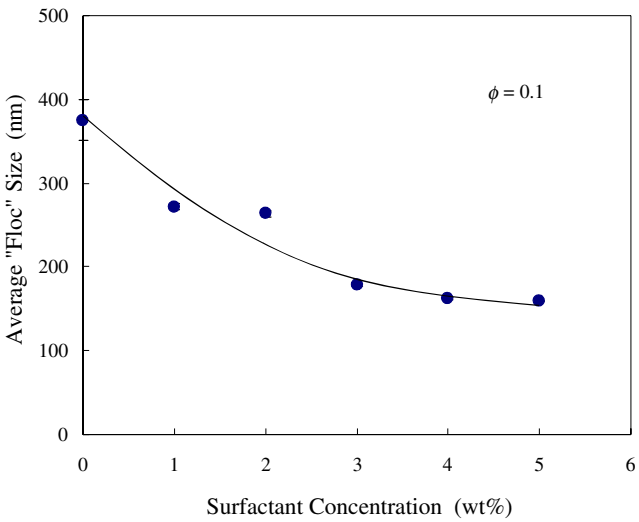

Fig. 5 The mean "floc" size of $BaTiO_3$ nanoparticle suspensions determined from the dynamic light scattering method at various surfactant concentrations. The solids concentration was held at ϕ=0.1

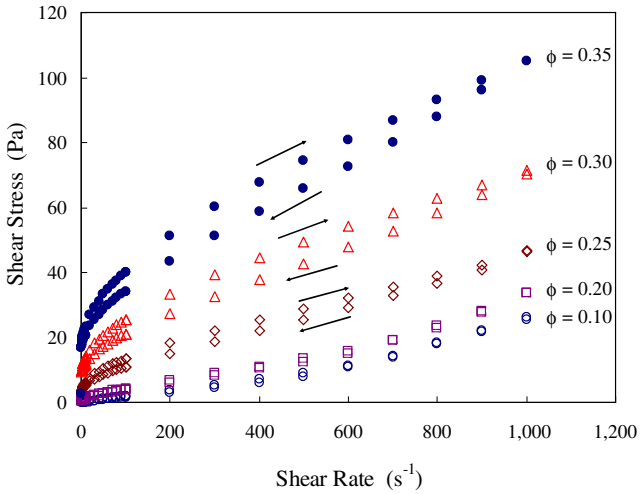

Fig. 6 Shear stress (τ)—shear rate ($\dot{\gamma}$) dependence of the $BaTiO_3$ nanoparticle suspensions. The surfactant concentration was held at 3 wt.%

change of macroscopic flow behavior is attributed to a microstructural order–disorder transition or cluster formation in the nanoparticle suspensions when shear rate alters [18]. Barnes [21] showed that when an externally applied shear force is able to break apart the interparticle bonds of powdered agglomerates, a formation of densely packed particle configuration would become energetically favorable for powdered suspensions. This relatively compact packing structure with a reduced effective volume and a resultant homogeneous flow pattern lead to a decreased flow resistance; which in turn, facilitates the macroscopic flow. When shear rate exceeds a certain critical level, the intricate balance between the densely packed particles becomes sensitive to any perturbation (such as irregular particle shape, particle-size distribution, surface morphology of particles, etc.) existing in the flowing suspensions. The perturbation increases particle interference and transforms the suspension structure into a three-dimensional, voluminous particle configuration at high shear rates, requiring then a greater shear stress to deform.

In Fig. 6, yield stress of the nanoparticle suspensions begins to appear as $\phi \geq 0.20$, and becomes prominent as $\phi \geq 0.25$. The magnitude of τ_y is related to the linkage of bonded molecules and particles of the suspensions network; therefore, τ_y is the stress required to overcome the chain-like bonding of the suspensions to initiate flow. Two empirical models are used in the study to determine τ_y [16]:

$$\text{Casson model}: \quad \tau^{1/2} = \tau_{y,c}^{1/2} + \left(\eta_s \dot{\gamma}\right)^{1/2} \tag{1}$$

$$\text{Herschel} - \text{Bulkley model}: \quad \tau = \tau_{y,h} + K \dot{\gamma}^{n} \tag{2}$$

where $\tau_{y,c}$ and $\tau_{y,h}$ are yield-stress parameters determined from the Casson and Herschel–Bulkley models, respectively; K and n are structure-dependent parameters that can be determined experimentally. As shown in Table 1, τ_y appears to increase disproportionately with ϕ when $\phi \geq 0.25$, regardless of the models used. The τ_y values are compared to the interparticle separation of the nanoparticle suspensions. The mean surface-to-surface separation (h) of particle-filled suspensions is related to the particulate volume fraction (ϕ) [22]:

$$\frac{h}{a} = 2\left[\left(\frac{\phi_{max}}{\phi}\right)^{1/3} - 1\right] \tag{3}$$

where a is the particle radius. The maximum packing fraction ϕ_{max} is typically in a range of 0.58–0.71, depending on the particle shape, particle-size distribution and shear rate examined [23]. By assuming ϕ_{max} equals to 0.64, which corresponds to that of the random close packing of mono-sized spheres, the disproportionate increase of τ_y with ϕ is transformed to $\tau_y - h$ relationship in Table 1. The suspension τ_y appears to become pronounced as the interparticle separation h is reduced to a distance less than the particle radius of $BaTiO_3$ nanoparticles ($a \sim 30$ nm from Fig. 1).

The concentrated suspensions ($\phi \geq 0.25$) appear thixotropic in Fig. 6. This reveals that the concentrated suspensions are

Table 1 Yield stresses of the $BaTiO_3$ nanoparticle suspensions determined from empirical models.

ϕ	Yield stress τ_y (Pa)		h (nm)	ϕ_{eff} [a]	h_{eff} [b] (nm)
	Casson model	Herschel–Bulkley model			
0.10	0	0	51	0.16	1.19
0.20	0.3	0.8	28	0.32	0.53
0.25	4.1	6.1	22	0.40	0.35
0.30	10.3	13.6	17	0.48	0.21
0.35	17.8	21.5	13	0.56	0.10

h Represents the average interparticle separation calculated from Eq. 3 by assuming $\phi_{max}=0.64$.
[a] ϕ_{eff} is calculated from Eq. 4 assuming the adsorbed surfactant thickness is 5 nm.
[b] h_{eff} is calculated from Eq. 5.

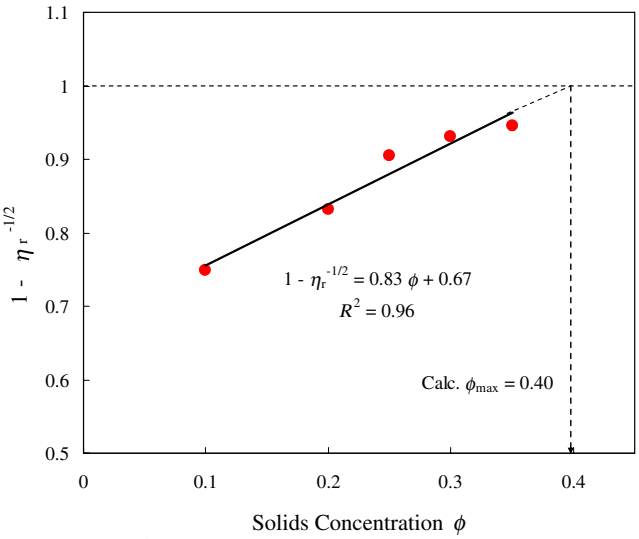

Fig. 7 $1-\eta_r^{-1/2}$ values appear to be linearly proportional to ϕ for the $BaTiO_3$ nanoparticle suspension

flocculated in character despite presence of the surfactant molecules. The mean floc size of the concentrated suspensions is expected to reduce in compliance with the shear-rate increase. Re-clustering of the floc assemblies, however, requires time to "resume" their original state at given shear rate before the disintegration. This leads to a relatively reduced stress level when shear rate is in the decreasing mode.

By using a model proposed by Liu [23], the theoretical, maximum solids fraction (ϕ_{max}) achievable for the $BaTiO_3$ nanoparticle suspensions is determined experimentally. The model uses a derivative of relative viscosity (η_r), i.e., $1-\eta_r^{-1/2}$; to which, a linear relationship of the $1-\eta_r^{-1/2}$ with ϕ appears valid in powder suspensions over a broad range of particle size, particle-size distribution and composition. Figure 7 shows the linear dependence of the $1-\eta_r^{-1/2}$ values to ϕ with a reasonable correlation factor R^2=0.96 over the solids-loading range examined ($\phi = 0.1-0.35$). ϕ_{max} is then determined from extrapolating the fitted line to $1-\eta_r^{-1/2}=1$, corresponding to η_r approaches infinity. This gives ϕ_{max}=0.40 for the model $BaTiO_3$ suspensions at a shear rate often encountered in most tape-casting operations ($\dot{\gamma} = 100\ s^{-1}$). Note that the experimentally determined ϕ_{max} is substantially lower than that of the random close packing of monosized spheres (ϕ_{max}~0.64). This is in part due to the particle interactions involved in the powdered suspensions. In addition, the reduced physical size of the $BaTiO_3$ nanoparticles is also of critical importance. In our earlier study [14], ϕ_{max} of submicrometer-sized $BaTiO_3$ suspensions was determined as ϕ_{max}=0.62 in carrier liquids of identical solvent and surfactant system. When one takes account of the volume occupied by the preferentially adsorbed surfactant molecules to the solids fraction of the suspensions, an "effective" solids concentration (ϕ_{eff}) is expected to be greater than ϕ and this increase becomes more pronounced as the particle size is reduced. ϕ_{eff} of mono-sized powder suspensions is estimated as [5, 18]:

$$\phi_{eff} = \phi(1+\delta/a)^3 \tag{4}$$

where δ is the adlayer thickness around the particle surface. At a first approximation, we take ϕ_{eff}=0.64, a=30 nm, and ϕ=0.40 (i.e., the calculated ϕ_{max} in Fig. 7) into Eq. 4, the calculated δ then equals to 5 nm. Table 1 lists the calculated ϕ_{eff} when the adlayer thickness δ is taken as 5 nm for all the solids concentrations examined. The calculated ϕ_{eff} is enhanced pronouncedly by the volume occupied by the "soft" layer around each particle. The "effective" interparticle spacing (h_{eff}) taken into account the adsorbed molecules thickness can then be solved by re-writing Eq. 3:

$$\frac{h_{eff}}{a} = 2\left[\left(\frac{\phi_{max}}{\phi_{eff}}\right)^{1/3} - 1\right] \tag{5}$$

The calculated h_{eff} values are shown in Table 1 by assuming ϕ_{max}=0.64. The h_{eff} values are dramatically reduced from the nominal h values because of the adsorbed surfactant layer. Moreover, the calculated h_{eff} reduces to a minimum of 0.1 nm for the highly concentrated suspension (i.e., ϕ_{eff}=0.56), suggesting that a suspension structure approaching the closest packing of spherical "particles" in solvents is attained. Even though the validity of the calculated h_{eff} remains to be seen because of the estimate of the adlayer thickness as well as the monosized, spherical particle shape assumed, powdered suspensions with particles in close proximity can virtually be regarded as a "pseudo-solid" since a continuous particulate network is formed in the highly flocculated state. As a result, the network prohibits the suspension from deformation at ease. This explains why the theoretical ϕ_{max} can only reach 0.40 in our nanoparticle suspension system examined. However,

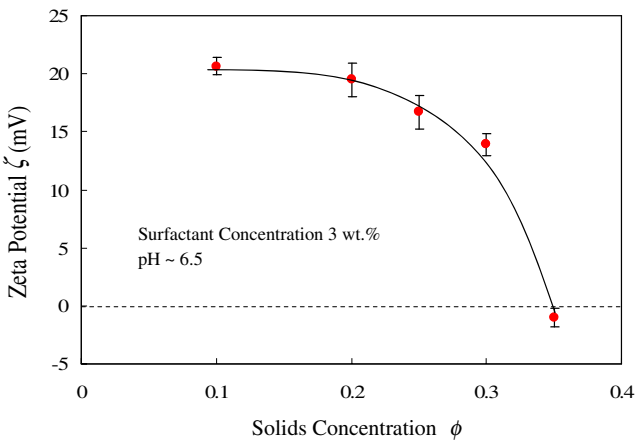

Fig. 8 The dependence of zeta potential with solids concentration for the model $BaTiO_3$-ethanol isopropanol suspensions

it is difficult to justify the calculated effective interparticle separation h_{eff} since the molecular structure, conformation and molecular weight of the commercial surfactant used in the study are unknown to the authors. The above calculations are thus speculative, yet state the importance of surfactant adsorption to the effective solids concentration and the suspension properties.

It may be interesting to note that zeta potential (ζ) of our $BaTiO_3$ nanoparticle suspensions decreases with the increasing solids concentration ($\phi = 0.10 - 0.35$) in the solvent mixtures (Fig. 8). The surface potential appears to decrease as ϕ exceeds ~0.15 and reaches a net zero charge when ϕ approaches 0.35. This finding combining with the calculated effective interparticle separation (h_{eff}~0.1 nm for suspensions of ϕ=0.35 in Table 1) may explain the formation of continuous particulate network in the carrier solvent as the solids concentration approaches toward the theoretical $\phi_{\max}$ value. In addition, Fig. 8 also suggests that the electrostatic part of the interparticle repulsions may be equally important with the steric hindrance in determining the stability of $BaTiO_3$ nanoparticles in organic solvents of low dielectric constant. This finding may provide a first known, direct evidence to support the propositions made earlier by Paik et al. [10]. Note that the crowded effect (from the increase of solids fractions) cannot be expected to operate in a substantial extent since dilute dispersions from the centrifuged, concentrated suspensions were prepared for the ζ measurement. We suspect that the reduced zeta potential is probably due to the dissolution of barium ions from the $BaTiO_3$ particle surface. The presence of ionic species in the carrier liquids would compress the electrical double layer around the particle surface, giving rise to the reduced zeta potential. Nonionic polyoxyethylene-based surfactants have been known to be rather insensitive to the presence of electrolyte, electrolyte concentration, and solution pH. The free Ba^{2+} ions in solution are hence expected not to influence the preferential adsorption of the surfactant molecules on polar particle surface. Therefore, the inevitable reduction of the effective interparticle separation together with the dramatic change of electrostatic potential on the particle surface both contribute to the degradation of suspension stability as the solids concentration approaches its maximum.

Paik and Hackley [24] have reported an increasing dependence of electrokinetic mobility with solids concentration at pH values below the pH_{IEP} of aqueous $BaTiO_3$ suspensions, which is different from our findings. Exact mechanisms are not clearly understood. Nonetheless, given the different solvent systems used in the studies and the solids-concentration range examined (ϕ=0.00005 to 0.05 for Paik and Hackley [24], and ϕ=0.1 to 0.35 in this study) we suspect that complex interactions and reactions involved in $BaTiO_3$-water and $BaTiO_3$-ethanol interface would possibly play critical roles at different solids fractions so that various mechanisms are responsibly operative.

4 Conclusions

An oxyethylene-based polymeric surfactant of non-ionic nature facilitates the dispersion of $BaTiO_3$ nanoparticles in ethanol–isopropanol solvents, leading to pronounced reduction in suspension viscosity. The improved dispersion is originated partly from the formation of preferentially adsorbed polymeric layers on the particle surface so that steric hindrance is operative to avoid direct particle contacts and the formation of agglomerations. The dispersion is also partly attributed to the positively charged $BaTiO_3$ particles which give rise to an additional electrostatic, interparticle repulsion in given solvent mixtures when the particles are brought into close proximity. Increase of the solids concentration leads to an increased instability of the suspensions. Theoretically determined maximum solids fraction is $\phi_{\max}$=0.40 at $\dot{\gamma} = 100\ s^{-1}$, which is markedly lower than that of the submicrometer counterpart in identical solvent and surfactant systems. We suspect that the decrease of the effective interparticle separation and the repulsive electrostatic potential contributes to the degradation of suspension stability.

Acknowledgments Financial support from the National Science Council (Taiwan, R.O.C.) under contract NSC 92-2216-E-005-020, and from the Advanced Green Energy Materials Project of the National Chung Hsing University from a special grant of the Ministry of Education are acknowledged.

References

1. S.K. Bhattacharya, R.R. Tummala, J. Mater. Sci., Mater. Electron. **11**, 253 (2000)
2. Z.-C. Chen, T.A. Ring, J. Lemaître, J. Am. Ceram. Soc. **75**, 3201 (1992)
3. J.-H. Jean, H.-R. Wang, J. Am. Ceram. Soc. **83**, 277 (2000)
4. K.-C. Hsu, K.-L. Ying, L.-P. Chen, B.-Y. Yu and W.-C. J. Wei, J. Am. Ceram. Soc. **88**, 524 (2005)
5. R.J. Pugh, L. Bergström, *Surface and Colloid Chemistry in Advanced Ceramics Processing* (Marcel Dekker, New York, 1994), p. 294
6. A.W.M. de Laat, W.P.T. Derks, Colloid Surf., A **71**, 147 (1993)
7. T. Chartier, E. Jorge, P. Boch, J. Eur. Ceram. Soc. **11**, 387 (1993)
8. F.M. Fowkes, M.A. Mostafa, Ind. Eng. Chem. Prod. Res. Dev. **17**, 3 (1978)
9. K. Mikeska, W.R. Cannon, Colloid Surf. **29**, 305 (1988)
10. U. Paik, V.A. Hackley, S.-C. Choi, Y.-G. Jung, Colloid Surf., A **135**, 77 (1998)
11. S. Bhattacharjee, M.K. Paria, H.S. Maiti, J. Mater. Sci. **28**, 6490 (1993)
12. W.J. Tseng, C.L. Lin, Mater. Lett. **57**, 223 (2002)
13. C.W. Cho, Y.S. Cho, J.G. Yeo, J. Kim, U. Paik, J. Eur. Ceram. Soc. **23**, 2315 (2003)

14. W.J. Tseng, C.L. Lin, Mater. Chem. Phys. **80**, 232 (2003)
15. Z.-G. Shen, J.-F. Chen, H.-K. Zou, J. Yun, Colloid Surf., A **244**, 61 (2004)
16. J.S. Reed, *Principles of Ceramics Processing* (Wiley, New York, 1995), p. 403
17. W.J. Tseng, S.-Y. Lin, S.-R. Wang, J. Electroceram. **16**, 537 (2006)
18. J.A. Lewis, J. Am. Ceram. Soc. **83**, 2341 (2000)
19. B. Lee, J. Zhang, Thin Solid Films **388**, 107 (2001)
20. O. Harizanov, A. Harizanova, T. Ivanova, Mater. Sci. Eng., B **106**, 191 (2004)
21. H.A. Barnes, J. Rheol. **33**, 329 (1989)
22. N.J. Wagner, J.W. Bender, MRS Bull. **29**, 100 (2004)
23. D.-M. Liu, J. Mater. Sci. **35**, 5503 (2000)
24. U. Paik, V.A. Hackley, J. Am. Ceram. Soc. **83**, 2381 (2000)